HHS Public Access

Author manuscript

Science. Author manuscript; available in PMC 2020 March 10.

Published in final edited form as:

Science. 2019 August 30; 365(6456): 929–934. doi:10.1126/science.aaw5937.

Membrane-associated periodic skeleton is a signaling platform for RTK transactivation in neurons

Ruobo Zhou[1,2,3], **Boran Han**[1,2,3], **Chenglong Xia**[1,2,3], **Xiaowei Zhuang**[1,2,3,*]

[1]Howard Hughes Medical Institute, Harvard University, Cambridge, MA 02138, USA.

[2]Department of Chemistry and Chemical Biology, Harvard University, Cambridge, MA 02138, USA.

[3]Department of Physics, Harvard University, Cambridge, MA 02138, USA.

Abstract

Actin, spectrin and associated molecules form a membrane-associated periodic skeleton (MPS) in neurons. The function of the MPS, however, remains poorly understood. Using super-resolution imaging, we observed that G-protein coupled receptors (GPCRs), cell-adhesion molecules (CAMs), receptor tyrosine kinases (RTKs), and related signaling molecules were recruited to the MPS in response to extracellular stimuli, resulting in colocalization of these molecules and RTK transactivation by GPCRs and CAMs, giving rise to extracellular-signal-regulated kinase (ERK) signaling. Disruption of the MPS prevented such molecular colocalizations and downstream ERK signaling. ERK signaling in turn caused calpain-dependent MPS degradation, providing a negative feedback that modulates signaling strength. These results reveal an important functional role of the MPS and establish it as a dynamically regulated platform for GPCR- and CAM-mediated RTK signaling.

One Sentence Summary

The actin-spectrin-based periodic membrane skeleton coordinates signal transduction in neurons.

Signal transduction mediated by cell surface receptors requires precise coordination of a cascade of molecular events. Receptor tyrosine kinases (RTKs) constitute a large class of such cell surface receptors that are expressed across many cell types and perform a broad spectrum of cellular functions, including promotion of cell survival, regulation of cell division and differentiation, and modulation of cellular metabolism and cell-to-cell communication (1, 2). RTKs are activated in response to extracellular signals, initiating a number of intracellular signal transduction cascades to alter gene expression in cells (1–4). The kinase activity of RTK can be activated either directly by their cognate ligands or through transactivation by other transmembrane proteins (1, 2, 4–7). Among the RTK

*Correspondence to: zhuang@chemistry.harvard.edu (X.Z.).

Author contributions: R.Z. and X.Z. designed the experiments. R.Z. and C.X. performed the experiments. R.Z. and B.H. performed data analysis. R.Z. and X.Z. wrote the manuscript with input from B.H. and C.X.

Competing financial interests: The authors declare no competing financial interests.

Data and materials availability: All data are available in the manuscript or supplementary materials.

transactivators are G-protein coupled receptors (GPCRs), the largest class of cell surface receptors in eukaryotes, and cell-adhesion molecules (CAMs), the class of transmembrane proteins responsible for cell-cell interactions (1, 4–7). In neurons, RTK transactivation by GPCRs and CAMs, as well as direct activation of RTKs by their cognate ligands, play important roles in regulating neurite outgrowth and axon guidance, controlling neuronal migration and repair, and modulating synaptogenesis and synaptic transmission (3–8). However, it is largely unknown how GPCRs, CAMs, RTKs and related signaling components are spatially organized at the neuronal cell surface and how these molecules are brought together to enable RTK transactivation and downstream signaling.

Recently, it has been shown that actin, spectrin and associated molecules form a membrane-associated periodic skeleton (MPS) structure in the axons and dendrites of neurons (9–12). The neuronal MPS contains molecular components homologous to those of the erythrocyte membrane skeleton (13), but adopts a distinct ultrastructure: in neurites, actin filaments are assembled into ring-like structures that are periodically spaced by spectrin tetramers, forming a quasi-one-dimensional lattice structure underneath the plasma membrane with a periodicity of ~190 nm (9). This structure is present in distinct types of neurons and across diverse animal species (14, 15). The MPS can organize transmembrane proteins, such as ion channels and adhesion molecules, into periodic distributions along axons (9, 11, 16–18), raising the possibility that this submembrane lattice structure may mediate membrane-associated signal transduction by regulating the distributions of related signaling proteins in space and time.

To test this hypothesis, we applied stochastic optical reconstruction microscopy (STORM) (19, 20), a super-resolution imaging method, to examine the spatial distributions of two transmembrane proteins that are known to transactivate RTKs in neurons (5, 7, 21, 22): i) the cannabinoid type 1 receptor (CB1), the most abundant GPCR in the brain and a therapeutic target for regulating appetite, pain, mood and memory, and for treating neurodegenerative diseases (23), and ii) the neural cell adhesion molecule 1 (NCAM1), a immunoglobulin superfamily CAM important for neuronal migration, neurite outgrowth and fasciculation, and neural circuit development (7). We used two-color STORM to investigate the spatial relationship between the MPS and these membrane proteins in cultured hippocampal neurons (Fig. 1). The MPS was visualized through immunolabeling of the C-terminus of βII-spectrin, which is located at the center of each spectrin tetramer connecting adjacent actin rings and is near the binding site for ankyrin, an adaptor protein that can connect transmembrane proteins to the membrane skeleton (13, 24).

Before stimulation with exogenous ligands, CB1 and NCAM1 exhibited a small degree of colocalization with the C-terminus of βII-spectrin, i.e. the center of the spectrin tetramer, in axons (Fig. 1, A and C, left). We quantified the degree of colocalization using one-dimensional (1D) cross-correlation analysis by projecting the signals to the longitudinal axis of the axon and calculating the average 1D cross-correlation function between the two color-channels over many axon segments. The 1D cross-correlation amplitude, defined as the average amplitude of the peaks at ±190 nm (the period of the MPS), quantifies not only the colocalization between the signaling molecules and the MPS, but also the degree of periodicity of these signaling molecules (Fig. 1, B and D, blue). The observed average cross-

correlation amplitudes were >10 fold greater than the values derived from single-color-labeled neurons, indicating that the observed colocalization was not due to crosstalk between the two color-channels (fig. S1). Notably, upon treatment with ligands, a CB1 agonist WIN 55,212–2 (WIN, Ki = 62 nM) (23) or a NCAM1 antibody (NCAM1 Ab) that binds to the extracellular domain to mimic homophilic or heterophilic binding of NCAM (7), CB1 or NCAM1 respectively displayed a substantially higher degree of colocalization with the MPS (Fig. 1, A and C, middle) with a 3–4 fold increase in the cross-correlation amplitudes (Fig. 1, B and D, red), and a significant reduction in the average distance between CB1/NCAM1 and their nearest-neighbor spectrin tetramer centers(fig. S2). Quantitatively similar ligand-induced increase in colocalization between CB1/NCAM1 and the MPS was observed using different cell fixation protocols (fig. S3). Such colocalization was abolished by treatment with actin depolymerizing drugs latrunculin A (LatA) and cytochalasin D (CytoD) (Fig. 1, A and C, right; B and D, yellow), which is known to disrupt the MPS structure (10, 12). Together, these results indicate ligand-induced recruitment of CB1 and NCAM1 to the MPS. Further supporting this notion, co-immunoprecipitation experiments also showed increased interaction of CB1 and NCAM1 with the MPS upon ligand treatment (fig. S4).

Next, we tested whether the recruitment of CB1 and NCAM1 to the MPS is important for the downstream signaling. It has been shown that, upon ligand binding, both CB1 and NCAM1 can activate the Raf-MEK-ERK signaling cascade through RTK transactivation in neurons (Fig. 2A) (7, 22). We thus measured the level of phosphorylated (activated) ERK (pERK) using an immunofluorescence assay (25) to quantify the signaling strength. Upon treatment with either the CB1 agonist WIN or the NCAM1 Ab, we observed a transient increase in pERK signal in neurons, followed by a decay to basal levels (Fig. 2, B and C, blue), consistent with previous reports (22, 26). Similar ERK activation was observed regardless of whether the analysis was done for axons only or for all neurites (fig. S5). Pretreating the neurons with a CB1-specific antagonist SR141716 (SR, Ki = 2 nM) that has little activity on CB2 (27–29) abolished the observed WIN-induced pERK signal increase in neurons (Fig. 2C, green), as well as the WIN-induced increase in CB1 and MPS colocalization (Fig. 1B, green).

Notably, disruption of the MPS structure by the LatA/CytoD treatment completely abolished the transient, ligand-induced ERK activation (Fig. 2C, yellow). Similar results were obtained by βII-spectrin knockdown (Fig. 2C, red, and 2D), which is also known to disrupt the MPS structure (10, 12). The cell-surface expression levels of CB1 and NCAM1 did not decrease in βII-spectrin knockdown neurons (fig. S6), excluding the possibility that the knockdown effect on ERK activation was due to a decrease in the surface expression of CB1 or NCAM1. Similar βII-spectrin-dependent, ligand-induced ERK activation was also observed using Western blot analysis (fig. S7). Together, these results suggest that the MPS plays an important role in enabling the CB1- and NCAM1-mediated ERK signaling.

Next, we investigated mechanistically how CB1- or NCAM1-mediated ERK signaling is facilitated by the MPS. To this end, we first examined which step along the signaling pathway is affected by MPS disruption. Both CB1- and NCAM1-mediated RTK transactivations activate protein kinase C (PKC), which in turn activates the ERK cascade in neurons (Fig. 2A) (5, 7, 22). We thus added PDBu, a direct PKC activator, to neurons and

measured the resulting pERK signal. The PDBu-induced increase in pERK signal was not diminished by βII-spectrin knockdown (fig. S8A), indicating that the MPS did not act directly on the Raf-MEK-ERK cascade downstream of PKC. Previous studies (5, 7, 21, 22) have suggested that CB1 and NCAM1 can transactivate two RTKs in neurons, tropomyosin receptor kinase B (TrkB) and fibroblast growth factor receptors (FGFR). Indeed, the addition of TrkB and FGFR inhibitors, and likewise the knockdown of TrkB and FGFR1, strongly suppressed the increase in pERK signal induced by WIN or NCAM1 Ab (fig. S8, B and C). These results indicate that the ERK signaling in neurons induced by CB1 and NCAM1 ligands was primarily through transactivation of the two RTKs, TrkB and FGFR. To test whether MPS facilitates CB1- and NCAM1-mediated transactivation of these two RTKs or events downstream of TrkB and FGFR activation, we examined whether MPS disruption inhibits the TrkB and FGFR activation induced directly by their own cognate ligands, brain-derived neurotrophic factor (BDNF) for TrkB and basic fibroblast growth factor (bFGF) for FGFR. The pERK signal increase induced by BDNF or bFGF remained quantitatively similar in βII-spectrin knockdown neurons as compared to wild type neurons (fig. S8, D and E), suggesting that the MPS does not act downstream of these RTKs, but likely affects their transactivation by CB1 and NCAM1. Indeed, using Western blot analysis, we observed activation (phosphorylation) of TrkB and FGFR upon addition of the CB1 ligand WIN, as well as activation of FGFR by the NCAM1 Ab treatment, both in a βII-spectrin-dependent manner (Fig. 2, E and F).

Next, we used STORM to examine the spatial relationship of the two RTKs, TrkB and FGFR1, to the MPS, as well as to the RTK transactivators, CB1 and NCAM1. Upon addition of WIN, both RTKs displayed a substantial increase in colocalization with the MPS, reflected by a 3–5 fold increase in 1D cross-correlation amplitudes, and disruption of the MPS by LatA/CytoD treatment abolished these colocalizations (Fig. 3A). Co-imaging of CB1 with TrkB or FGFR1 showed little colocalization between these molecules before addition of WIN, whereas the amplitude and periodicity of the 1D cross-correlation functions increased dramatically upon WIN addition (Fig. 3B), suggesting ligand-induced colocalizations between CB1 and the two RTKs. MPS disruption by LatA/CytoD treatment or βII-spectrin knockdown completely eliminated this ligand-induced colocalization (Fig. 3B). One potential caveat of this 1D analysis is that the increase in the 1D cross-correlation may be only a reflection of the recruitment of both CB1 and RTKs to the MPS, and may not necessarily indicate an enhanced spatial proximity between CB1 and RTKs themselves. We thus performed 2D cross-correlation analysis between CB1 and the two RTKs (fig. S9A), as well as nearest-neighbor distance analysis between these molecules (fig. S9B), to further probe their colocalization. Both analyses showed that WIN treatment indeed enhanced proximity between CB1 and the two RTKs in an MPS-dependent manner. Similarly, NCAM1 Ab treatment also induced colocalization between NCAM1 and FGFR1 in an MPS-dependent manner (fig. S10). As an additional support, co-immunoprecipitation experiments showed that the interaction between CB1 and the two RTKs greatly increased upon WIN treatment, and likewise the interaction between NCAM1 and FGFR greatly increase upon NCAM1 Ab treatment, both in an MPS-dependent manner (fig. S11).

We further examined the spatial distributions of Src-family tyrosine kinases, which are known as important mediators of RTK transactivation by GPCRs and CAMs (Fig. 2A) (4–7,

30). As expected, preincubation with PP2, a specific Src-family kinase inhibitor, abolished the increase in pERK signal induced by CB1 and NCAM1 ligands in neurons (fig. S12). Notably, Src, a known mediator for GPCR-mediated RTK transactivation (4, 6), also became substantially more colocalized with the MPS upon WIN treatment, and this colocalization was abolished by MPS disruption (Fig. 3C). To test whether this recruitment of Src to the MPS depends on Src activity, we generated three Src mutants with different levels of kinase activities (Src^{Act}, Src^{SH2eng}, and $Src^{SH2-3eng}$) by introducing mutations that promote the open (active) or closed (inactive) conformation of Src (Fig. 3D) (31). The degree of colocalization between the MPS and these Src mutants scaled with their kinase activity in the absence of WIN, and the effect of WIN treatment on the Src-MPS colocalization was substantially reduced for the constitutively active mutant Src^{Act}, exhibiting only a 48% (instead of 3–4 fold) increase in 1D cross-correlation amplitude, and the WIN-induced increase was completely abolished for the two inactive Src mutants (Src^{SH2eng} and $Src^{SH2-3eng}$) (Fig. 3D and fig. S13). Likewise, Fyn, the Src-family kinase mediating NCAM1-induced RTK transactivation (30), also exhibited enhanced colocalization with the MPS upon NCAM1 Ab treatment (fig. S14).

Taken together, the above results suggest that the MPS acts as a signaling platform that brings CB1, NCAM1, RTKs and Src-family kinases into proximity to enable RTK transactivation by CB1 and NCAM1. Next, we investigated whether RTK transactivation and the downstream ERK signaling in turn have any effect on the MPS. Interestingly, after WIN or NCAM1 Ab treatment, the MPS was degraded gradually over time (Fig. 4, A and B; fig. S15, A and B). Preincubation with the CB1-antagonist SR blocked the WIN-induced MPS degradation (Fig. 4, A and C). Preincubation with U0126, an inhibitor (IC_{50} = 60–70 nM) of MEK, the kinase upstream of ERK (Fig. 2A), also protected the MPS from degradation (Fig. 4, A and C; fig. S15, A and C), indicating that the MPS degradation was a result of the ERK signaling. Brain spectrin is the substrate of the calpain protease (32) and RTK-induced ERK signaling activates calpain-2 (33), raising the possibility that the observed MPS degradation may be due to cleavage by calpain. Indeed, we found that inhibiting calpain activity with an inhibitor MDL-28170 (MDL, Ki = 8 nM) or shRNA against calpain-2 prevented signaling-induced MPS degradation (Fig. 4, A and C; fig. S15, A and C). With calpain or MEK activities inhibited and hence the MPS retained, the ligand-induced colocalization between signaling molecules and the MPS also maintained (fig. S16). These results indicate that CB1- and NCAM1-mediated RTK transactivation turns on an ERK-dependent calpain pathway that degrades the MPS. This degradation was reversible: the MPS structure reassembled within a few hours after ligand removal (fig. S17).

Because the MPS structure brings RTKs, RTK transactivators, and Src-family kinases into proximity to facilitate RTK transactivation, we envisioned that the MPS degradation could provide a negative feedback to reduce the strength of ERK signaling induced by RTK transactivation. Indeed, preventing MPS degradation by the calpain inhibitor MDL or calpain-2 knockdown increased ERK signaling induced by both WIN and NCAM1 Ab (Fig. 4, D and E; fig S15, D and E), supporting the existence of such a negative feedback loop.

Ligand binding could also induce receptor endocytosis, a process known to positively or negatively regulate various signaling pathways (34, 35). In addition to providing a platform

for recruiting signaling molecules, could the MPS influence the endocytosis of these molecules, which in turn also impacts ERK signaling? To examine whether the MPS affects CB1 endocytosis, we examined how the rate of ligand-induced CB1 endocytosis changed under two MPS perturbation conditions: 1) βII-spectrin knockdown, which disrupts the MPS, and 2) MDL treatment, which protects the MPS from signaling-induced degradation. βII-spectrin knockdown led to a substantial increase in WIN-induced CB1 endocytosis, whereas MDL treatment inhibited WIN-induced CB1 endocytosis (fig. S18), indicating that the MPS structure can repress endocytosis.

To estimate how much this effect of MPS on CB1 endocytosis would contribute to the observed negative feedback on signaling, we further examined the ERK signaling in clathrin heavy chain (CHC) knockdown neurons, as CB1 endocytosis is known to occur in a clathrin-dependent manner in neurons (36). Notably, although CHC knockdown inhibited CB1 endocytosis at least as strongly as MDL treatment did (fig. S18), it did not have a significant effect on ERK signaling induced by WIN (fig. S19), suggesting that the enhancement in ERK signaling observed under calpain inhibition (Fig. 4E) was not primarily due to inhibition of endocytosis. Hence, for CB1-mediated RTK transactivation, the negative feedback caused by the signaling-induced MPS degradation was likely a direct effect of the loss of the structural platform for signaling-molecule recruitment. Whether the same is true for NCAM1-mediated RTK transactivation remains to be investigated.

In summary, our results suggest that the MPS serves as a structural platform for bringing signaling molecules, including GPCRs, CAMs, RTKs, and Src-family kinases, into proximity to enable GPCR- and CAM-mediated transactivation of RTKs and the downstream ERK signaling (Fig. 4F). These signaling molecules were recruited to sites near the center of the spectrin tetramer, where the adaptor protein ankyrin binds. Both spectrin and ankyrin are large scaffolding proteins containing multiple domains, which could provide multiple binding sites for signaling molecules and bring them into proximity to form signaling complexes. Indeed, it has been shown that GPCR-signaling components, CAMs, and the Src kinase can interact with specific molecular domains of spectrin or ankyrin (13, 37, 38). It is also possible that some of these signaling molecules are first recruited to the MPS to increase their local concentration, which in turn facilitates the recruitment of other signaling molecules through multivalent interactions. In support of this view, optogenetically induced self-oligomerization of the SH2 domain, a common protein domain in many signaling molecules, including Src and Fyn kinases, has been shown to facilitate complex formation between RTKs and SH2, thereby activating RTKs (39). Our results thus raise the interesting possibility that MPS may facilitate multivalent-interaction-mediated phase separation of signaling molecules. Our observations of the recruitment of signaling molecules to the MPS upon ligand stimulation suggest a critical role of the MPS in signaling. Indeed, disruption of the MPS abolished ligand-induced RTK transactivation by CB1 or NCAM1, and the downstream ERK signaling. Furthermore, we demonstrated that the ERK signaling induced reversible MPS degradation in a calpain-protease-dependent manner, which in turn caused an attenuation of signaling strength, providing a negative feedback loop (Fig. 4F). In addition, we observed that MPS can regulate endocytosis, potentially providing another mechanism for signaling regulation. Taken together, our results demonstrate that the MPS functions as a dynamically regulated structural platform for

GPCR- and CAM-mediated RTK transactivation and signaling, providing a mechanism for regulating signal transduction in neurons.

Supplementary Material

Refer to Web version on PubMed Central for supplementary material.

Acknowledgements

We thank Dr. Hazen Babcock and Dr. Ye Fu for helping with two-color STORM imaging setup construction and data analysis, Dr. Ke Xu for providing the software for processing the two-color STORM imaging data, and Dr. Matthew Rasband for providing the adenoviruses expressing shRNA against βII-spectrin.

Funding: This work is supported in part by the National Institutes of Health. R.Z. is an HHMI Fellow of the Life Sciences Research Foundation. X.Z. is a Howard Hughes Medical Institute investigator.

References

1. Gschwind A, Fischer OM, Ullrich A, The discovery of receptor tyrosine kinases: targets for cancer therapy. Nat Rev Cancer 4, 361–370 (2004). [PubMed: 15122207]
2. Lemmon MA, Schlessinger J, Cell signaling by receptor tyrosine kinases. Cell 141, 1117–1134 (2010). [PubMed: 20602996]
3. Latham V, Singer RH, RNA Localization and Signal Transduction. Handbook of Cell Signaling 3, 293–297 (2003).
4. Cattaneo F et al., Cell-surface receptors transactivation mediated by g protein-coupled receptors. Int J Mol Sci 15, 19700–19728 (2014). [PubMed: 25356505]
5. Doherty P, Walsh FS, CAM-FGF receptor interactions: a model for axonal growth. Mol Cell Neurosci 8, 99–111 (1996).
6. Luttrell LM, Daaka Y, Lefkowitz RJ, Regulation of tyrosine kinase cascades by G-protein-coupled receptors. Curr Opin Cell Biol 11, 177–183 (1999). [PubMed: 10209148]
7. Ditlevsen DK, Povlsen GK, Berezin V, Bock E, NCAM-induced intracellular signaling revisited. J Neurosci Res 86, 727–743 (2008). [PubMed: 17975827]
8. Shen K, Cowan CW, Guidance molecules in synapse formation and plasticity. Cold Spring Harb Perspect Biol 2, a001842 (2010). [PubMed: 20452946]
9. Xu K, Zhong G, Zhuang X, Actin, spectrin, and associated proteins form a periodic cytoskeletal structure in axons. Science 339, 452–456 (2013). [PubMed: 23239625]
10. Zhong G et al., Developmental mechanism of the periodic membrane skeleton in axons. Elife 3, e04581 (2014).
11. D'Este E, Kamin D, Gottfert F, El-Hady A, Hell SW, STED nanoscopy reveals the ubiquity of subcortical cytoskeleton periodicity in living neurons. Cell Rep 10, 1246–1251 (2015). [PubMed: 25732815]
12. Han B, Zhou R, Xia C, Zhuang X, Structural organization of the actin-spectrin-based membrane skeleton in dendrites and soma of neurons. Proc Natl Acad Sci U S A 114, E6678–E6685 (2017). [PubMed: 28739933]
13. Bennett V, Lorenzo DN, An Adaptable Spectrin/Ankyrin-Based Mechanism for Long-Range Organization of Plasma Membranes in Vertebrate Tissues. Curr Top Membr 77, 143–184 (2016). [PubMed: 26781832]
14. D'Este E et al., Subcortical cytoskeleton periodicity throughout the nervous system. Sci Rep 6, 22741 (2016). [PubMed: 26947559]
15. He J et al., Prevalent presence of periodic actin-spectrin-based membrane skeleton in a broad range of neuronal cell types and animal species. Proc Natl Acad Sci U S A 113, 6029–6034 (2016). [PubMed: 27162329]
16. Albrecht D et al., Nanoscopic compartmentalization of membrane protein motion at the axon initial segment. J Cell Biol 215, 37–46 (2016). [PubMed: 27697928]

17. D'Este E, Kamin D, Balzarotti F, Hell SW, Ultrastructural anatomy of nodes of Ranvier in the peripheral nervous system as revealed by STED microscopy. Proc Natl Acad Sci U S A 114, E191–E199 (2017). [PubMed: 28003466]
18. Hauser M et al., The Spectrin-Actin-Based Periodic Cytoskeleton as a Conserved Nanoscale Scaffold and Ruler of the Neural Stem Cell Lineage. Cell Reports 24, 1512–1522 (2018). [PubMed: 30089262]
19. Rust MJ, Bates M, Zhuang X, Sub-diffraction-limit imaging by stochastic optical reconstruction microscopy (STORM). Nat Methods 3, 793–795 (2006). [PubMed: 16896339]
20. Huang B, Wang W, Bates M, Zhuang X, Three-dimensional super-resolution imaging by stochastic optical reconstruction microscopy. Science 319, 810–813 (2008). [PubMed: 18174397]
21. Berghuis P et al., Endocannabinoids regulate interneuron migration and morphogenesis by transactivating the TrkB receptor. P Natl Acad Sci USA 102, 19115–19120 (2005).
22. Asimaki O, Leondaritis G, Lois G, Sakellaridis N, Mangoura D, Cannabinoid 1 receptor-dependent transactivation of fibroblast growth factor receptor 1 emanates from lipid rafts and amplifies extracellular signal-regulated kinase 1/2 activation in embryonic cortical neurons. J Neurochem 116, 866–873 (2011). [PubMed: 21214560]
23. Howlett AC et al., International Union of Pharmacology. XXVII. Classification of cannabinoid receptors. Pharmacol Rev 54, 161–202 (2002). [PubMed: 12037135]
24. Huang CY, Rasband MN, Axon initial segments: structure, function, and disease. Annals of the New York Academy of Sciences 1420, 46–61 (2018). [PubMed: 29749636]
25. Krapivinsky G et al., The NMDA receptor is coupled to the ERK pathway by a direct interaction between NR2B and RasGRF1. Neuron 40, 775–784 (2003). [PubMed: 14622581]
26. Son H, Seuk Kim J, Mogg Kim J, Lee SH, Lee YS, Reciprocal actions of NCAM and tPA via a Ras-dependent MAPK activation in rat hippocampal neurons. Biochem Biophys Res Commun 298, 262–268 (2002). [PubMed: 12387826]
27. Hu S, Sheng WS, Rock RB, CB2 receptor agonists protect human dopaminergic neurons against damage from HIV-1 gp120. PLoS One 8, e77577 (2013). [PubMed: 24147028]
28. Robinson RH et al., Cannabinoids inhibit T-cells via cannabinoid receptor 2 in an in vitro assay for graft rejection, the mixed lymphocyte reaction. J Neuroimmune Pharmacol 8, 1239–1250 (2013). [PubMed: 23824763]
29. Rinaldicarmona M et al., Sr141716a, a Potent and Selective Antagonist of the Brain Cannabinoid Receptor. Febs Lett 350, 240–244 (1994). [PubMed: 8070571]
30. Maness PF, Schachner M, Neural recognition molecules of the immunoglobulin superfamily: signaling transducers of axon guidance and neuronal migration. Nat Neurosci 10, 19–26 (2007). [PubMed: 17189949]
31. Krishnamurty R et al., Active site profiling reveals coupling between domains in SRC-family kinases. Nat Chem Biol 9, 43–50 (2013). [PubMed: 23143416]
32. Kobeissy FH et al., Degradation of betaII-Spectrin Protein by Calpain-2 and Caspase-3 Under Neurotoxic and Traumatic Brain Injury Conditions. Mol Neurobiol 52, 696–709 (2015). [PubMed: 25270371]
33. Zadran S et al., Brain-derived neurotrophic factor and epidermal growth factor activate neuronal m-calpain via mitogen-activated protein kinase-dependent phosphorylation. J Neurosci 30, 1086–1095 (2010). [PubMed: 20089917]
34. Di Fiore PP, De Camilli P, Endocytosis and signaling. an inseparable partnership. Cell 106, 1–4 (2001). [PubMed: 11461694]
35. Sorkin A, von Zastrow M, Endocytosis and signalling: intertwining molecular networks. Nat Rev Mol Cell Biol 10, 609–622 (2009). [PubMed: 19696798]
36. Coutts AA et al., Agonist-induced internalization and trafficking of cannabinoid CB1 receptors in hippocampal neurons. J Neurosci 21, 2425–2433 (2001). [PubMed: 11264316]
37. Wang DS, Shaw R, Winkelmann JC, Shaw G, Binding of PH domains of beta-adrenergic receptor kinase and beta-spectrin to WD40/beta-transducin repeat containing regions of the beta-subunit of trimeric G-proteins. Biochem Biophys Res Commun 203, 29–35 (1994). [PubMed: 8074669]

38. Nedrelow JH, Cianci CD, Morrow JS, c-Src binds alpha II spectrin's Src homology 3 (SH3) domain and blocks calpain susceptibility by phosphorylating Tyr1176. J Biol Chem 278, 7735–7741 (2003). [PubMed: 12446661]

39. Bugaj LJ et al., Regulation of endogenous transmembrane receptors through optogenetic Cry2 clustering. Nat Commun 6, 6898 (2015). [PubMed: 25902152]

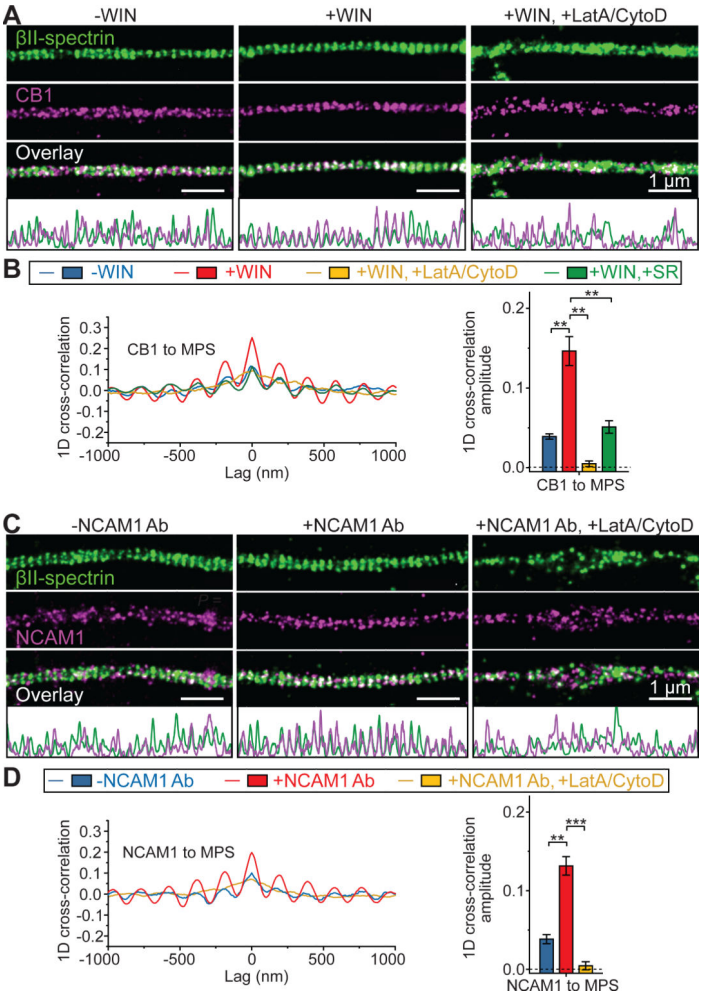

Fig. 1. CB1 and NCAM1 are recruited to the MPS upon cognate ligand binding.

(A) Two-color STORM images of βII-spectrin (green) and CB1 (magenta) in the axons of untreated neurons (left, "-WIN"), neurons treated with the CB1 agonist WIN (middle, "+WIN"), and neurons pretreated with LatA and CytoD to disrupt the MPS prior to addition of WIN (right, "+WIN, +LatA/CytoD"). 1D projection traces of βII-spectrin (green) and CB1 (magenta) signals along the axon are shown at the bottom. Scale bars: 1 μm. βII-spectrin was visualized by immunostaining with an antibody against the C-terminus of βII-spectrin. CB1 was visualized by immunostaining with CB1 antibody. **(B)** Left: Average 1D cross-correlation functions between the distributions of CB1 and βII-spectrin from many CB1-positive axon segments for the three conditions described in (A) as well as for neurons pretreated with the CB1 antagonist SR prior to addition of WIN ("+WIN, +SR"). Right: Average 1D cross-correlation amplitudes, defined as the difference between the average of the peaks at ± 190 nm and the average of the valleys at ± 95 nm and ± 285 nm of the average 1D cross-correlation functions. Blue: -WIN; Red: +WIN; Yellow: +WIN, +LatA/CytoD; Green: +WIN, +SR. **: $P < 0.01$; actual P values (from left to right): 4.4×10^{-3}, 1.6×10^{-3}, 8.7×10^{-3} (unpaired Student's t test). **(C, D)** Same as (A, B) but for neurons treated with NCAM1 antibody (NCAM1 Ab) instead of WIN. Neurons were pre-incubated with NCAM1 Ab at 4 °C to allow antibody binding in both "-NCAM1 Ab" and "+NCAM1 Ab"

conditions. NCAM1 Ab treatment ("+NCAM1 Ab") was achieved by a temperature increase to stimulate signaling (See Materials and Methods), whereas the temperature increase step was skipped in the "-NCAM1 Ab" condition to prevent signaling, as previously described (26). NCAM1 was visualized through immunostaining with the NCAM1 antibody. **: $P < 0.01$; ***: $P < 0.001$; actual P values (from left to right): 2.1×10^{-3}, 5.8×10^{-4} (unpaired Student's t test). Data in bar graphs are mean ± s.e.m. ($n = 3$ biological replicates; 100–200 axonal regions were examined per condition).

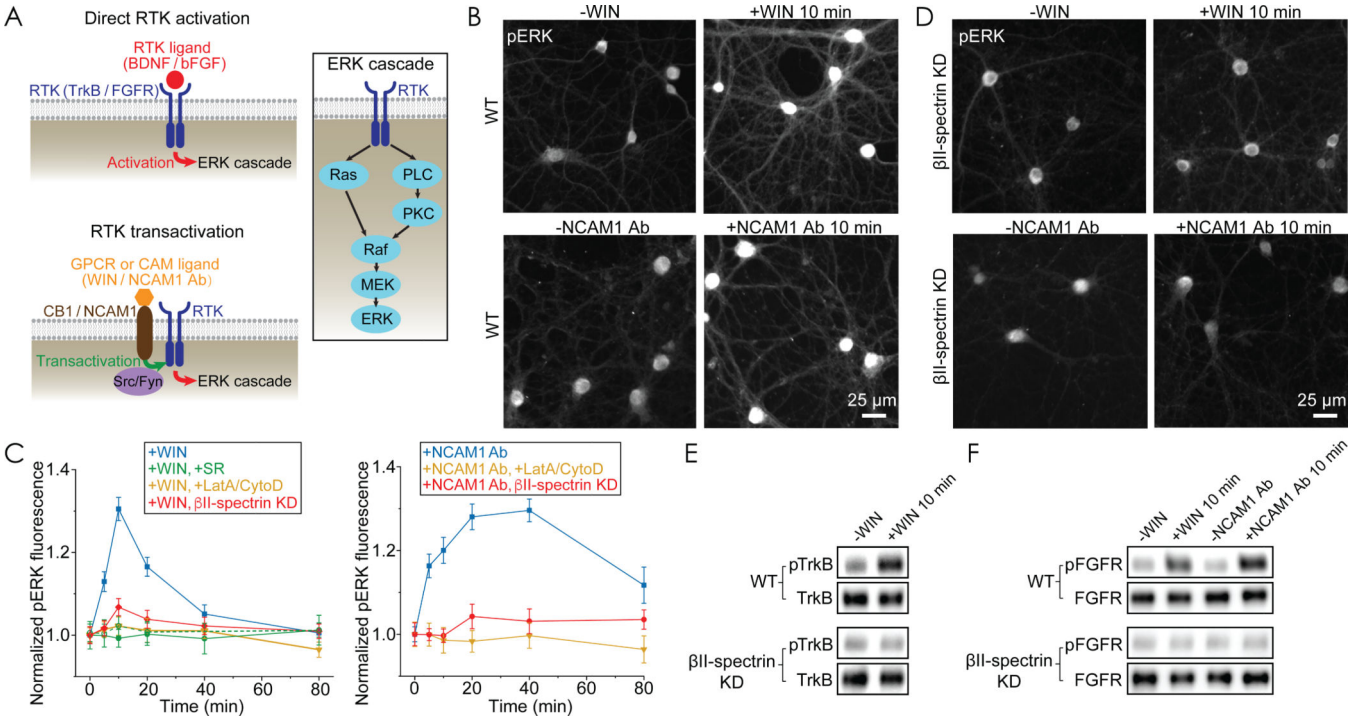

Fig. 2. MPS disruption abolishes RTK transactivation and downstream ERK signaling.

(A) Left: Diagrams showing direct RTK activation (top) and RTK transactivation (bottom). RTK can be either activated directly by binding of their cognate ligands or transactivated by other transmembrane proteins, such as CB1 (upon binding of CB1 ligand) and NCAM1 (upon binding of NCAM1 Ab). Right: Diagram showing the ERK signaling cascade downstream of RTK. PLC, phospholipase C. MEK, mitogen-activated protein kinase kinase. **(B)** Top: Immunofluorescence images of phosphorylated (activated) ERK (pERK) in wild type (WT) untreated neurons (left) and WT neurons treated with WIN for 10 min (right). WIN treatment was initiated by addition of WIN at 37 ºC. Bottom: Same as top but for treatment with NCAM1 Ab. Neurons were pre-incubated with NCAM1 Ab at 4 °C to allow antibody binding in both “-NCAM1 Ab” and “+NCAM1 Ab” conditions, and NCAM1 Ab treatment (“+NCAM1 Ab”) was then initiated by a temperature increase to 37 ºC, whereas this temperature increase step was eliminated in the “-NCAM1 Ab” condition to prevent signaling. Scale bar: 25 μm. **(C)** Time courses of ERK activation upon WIN addition (left) or upon NCAM1 Ab treatment (right) for WT neurons (blue), WT neurons pretreated with the CB1 antagonist SR (green, closed symbols: 1 μM SR; open symbols: 100 nM SR), WT neurons pretreated with LatA and CytoD (yellow), and βII-spectrin knockdown (KD) neurons (red). βII-spectrin KD was induced by adenovirus expressing βII-spectrin shRNA (fig. S6A). Data are mean ± s.e.m. (n = 3 biological replicates; 20–30 imaged regions were examined per condition). **(D)** Same as (B) but for βII-spectrin KD neurons instead of WT neurons. **(E)** Western blot analysis for phosphorylated (activated) TrkB (pTrkB) and total TrkB in whole-cell lysates from WT neurons (top) and βII-spectrin KD neurons (bottom) before and 10 min after WIN treatment. **(F)** Western blot analysis for phosphorylated (activated) FGFR (pFGFR) and total FGFR in whole-cell lysates from WT neurons (top) and βII-spectrin KD neurons (bottom) before and 10 min after the initiation of WIN or NCAM1

Ab treatment. Western blots are representative examples from two independent biological replicates.

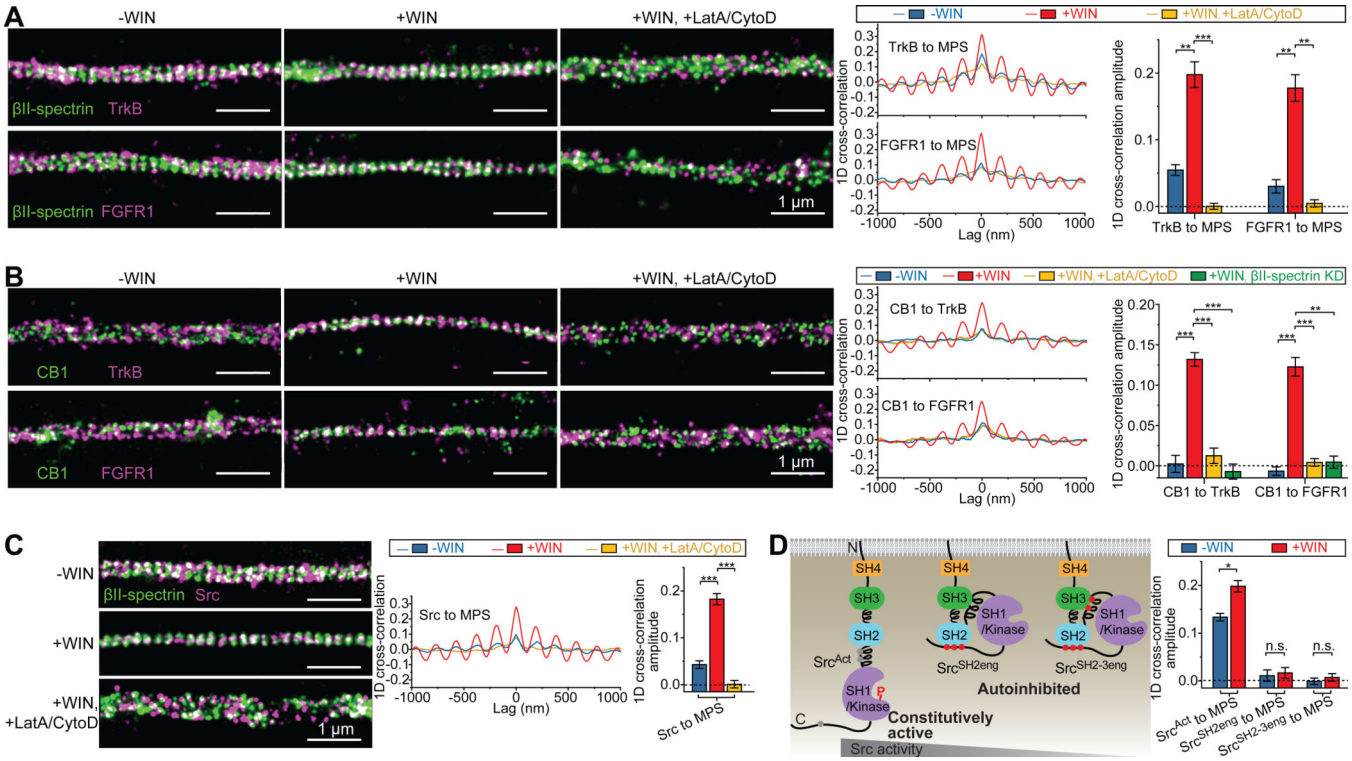

Fig. 3. The MPS functions as a signaling platform that brings RTKs, RTK transactivators and Src kinases into proximity.

(A) Left panels: Two-color STORM images of βII-spectrin (green) and TrkB (magenta) (top panels) and of βII-spectrin (green) and FGFR1 (magenta) (bottom panels) in CB1-positive axons of untreated neurons (left, "-WIN"), neurons treated with WIN (middle, "+WIN"), and neurons pretreated with LatA and CytoD prior to WIN addition (right, "+WIN, +LatA/CytoD"). Scale bars: 1 μm. Right panels: Average 1D cross-correlation functions and 1D cross-correlation amplitudes between the distribution of βII-spectrin and the distributions of RTKs (TrkB or FGFR1) from many CB1-positive axons for the three conditions. Blue: -WIN; Red: +WIN; Yellow: +WIN, +LatA/CytoD. **: $P < 0.01$; ***: $P < 0.001$; actual P values (from left to right): 2.3×10^{-3}, 5.6×10^{-4}, 2.8×10^{-3}, 1.2×10^{-3} (unpaired Student's t test). **(B)** Similar to (A) but for co-imaging of CB1, instead of βII-spectrin, with the two RTKs. The results for the +WIN condition in βII-spectrin KD neurons is additionally shown in green (+WIN, βII-spectrin KD). **: $P < 0.01$; ***: $P < 0.001$; actual P values (from left to right): 6.7×10^{-4}, 7.3×10^{-4}, 3.8×10^{-4}, 5.2×10^{-4}, 6.8×10^{-4}, 1.0×10^{-3} (unpaired Student's t test). **(C)** Similar to (A) but for co-imaging of Src with βII-spectrin. ***: $P < 0.001$; actual P values (from left to right): 6.4×10^{-4}, 2.2×10^{-4} (unpaired Student's t test). **(D)** Left: Diagram showing the intramolecular domain organizations of the three Src variants. Src^{Act} is a constitutively active mutant, and gray dots in Src^{Act} indicate the sites modified to disrupt the auto-inhibiting intramolecular domain interactions. Src^{SH2eng} and $Src^{SH2-3eng}$ are inactive mutants, and red dots in these mutants indicate the sites modified to facilitate the auto-inhibiting intramolecular domain interactions. The red "P" represents the major phosphorylation site of activated Src. Right: Average 1D cross-correlation amplitudes between the distributions of βII-spectrin and the three Src mutants. Blue: -WIN; Red:

+WIN. *: $P < 0.1$; n.s.: not significant ($P > 0.1$); actual P values (from left to right): 1.1×10^{-2}, 0.74, 0.49 (unpaired Student's t test). Data in bar graphs are mean ± s.e.m. ($n = 3$ biological replicates; 100–200 axonal regions were examined per condition). βII-spectrin and CB1 were visualized as described in Fig. 1; TrkB, FGFR1, and Src variants were visualized by moderate expression of GFP-tagged TrkB, FGFR1, or Src variants through low-titer lentiviral transfection and detection through GFP antibody.

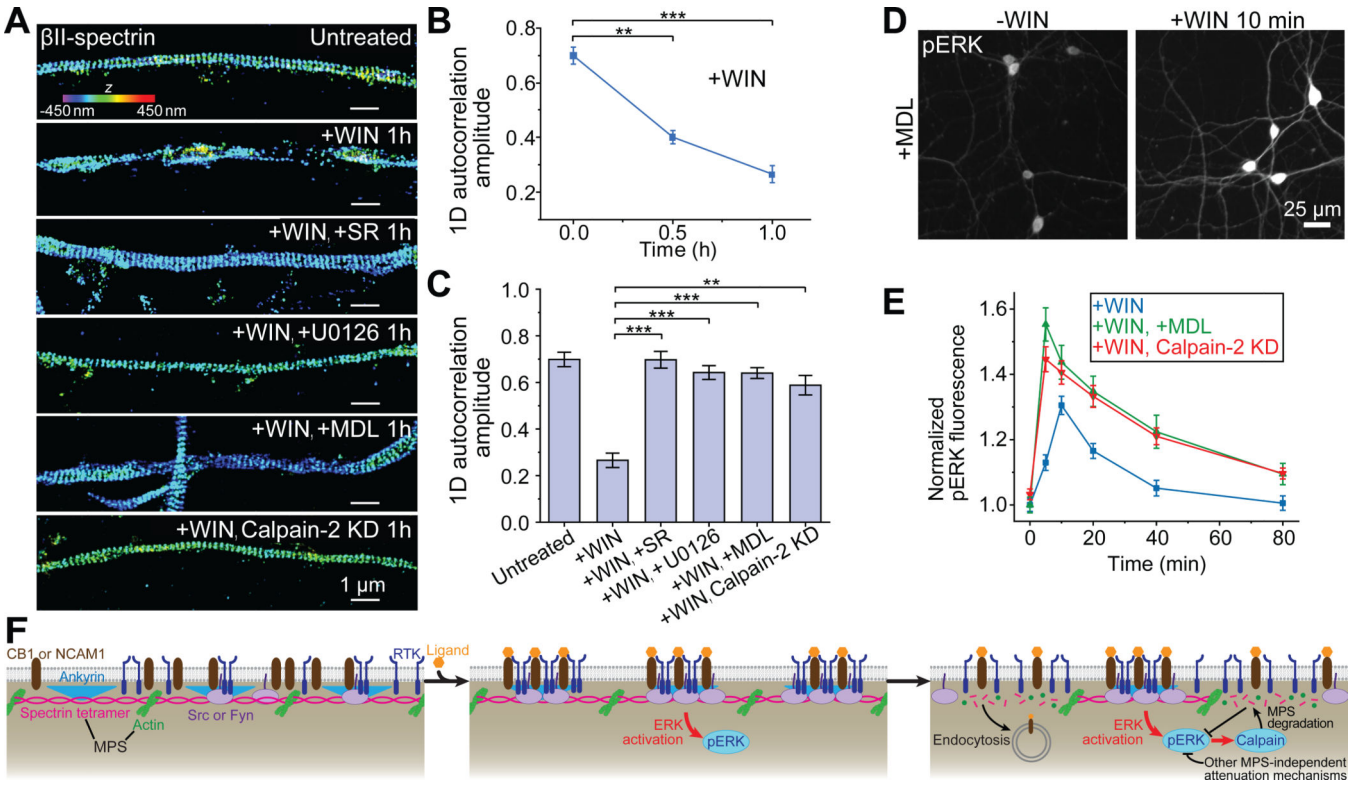

Fig. 4. ERK signaling causes disassembly of the MPS structure, providing a negative feedback for signaling.

(A) 3D STORM images of βII-spectrin in CB1-positive axons of untreated neurons, neurons treated with WIN for 1 hr in the absence and presence of SR (a CB1 antagonist), U0126 (a MEK inhibitor), MDL (a pan-calpain inhibitor), and calpain-2 KD neurons treated with WIN for 1hr. Calpain-2 KD was induced by adenovirus expressing calpain-2 shRNA (fig. S15A). Scale bars: 1 μm. Colored scale bar indicates the z-coordinate information. **: $P < 0.01$; ***: $P < 0.001$; actual P values (from left to right): 1.6×10^{-3}, 5.9×10^{-4} (unpaired Student's t test). **(B)** Average 1D auto-correlation amplitude of the βII-spectrin distribution, indicating the degree of the periodicity in the MPS, calculated from many axon segments at different time points after addition of WIN. **(C)** Average 1D auto-correlation amplitudes for the six conditions described in (A). **: $P < 0.01$; ***: $P < 0.001$; actual P values (from left to right): 8.0×10^{-4}, 9.2×10^{-4}, 6.3×10^{-4}, 3.5×10^{-3} (unpaired Student's t test). Data in (B) and (C) are mean ± s.e.m. ($n = 3$ biological replicates; 50–100 axonal regions were examined per condition). **(D)** Immunofluorescence images of activated ERK (pERK) in neurons pretreated with MDL, before (left) and after (right) WIN treatment. Scale bar: 25 μm. **(E)** Time courses of ERK activation upon addition of WIN for control neurons (blue), neurons pretreated with MDL (green), and calpain-2 knockdown neurons (red). The curve for control neurons is reproduced from Fig. 2C. Data are mean ± s.e.m. ($n = 3$ biological replicates; 20–30 imaged regions were examined per condition). **(F)** Schematic showing the MPS functioning as a dynamically regulated platform to recruit signaling molecules and enable RTK transactivation. Upon ligand binding to RTK transactivators (CB1 and NCAM1), these transactivators, RTKs (TrkB and FGFR), and related Src-family tyrosine kinases (Src and Fyn) are recruited to the MPS and brought into proximity of each other,

enabling RTK transactivation and the downstream ERK signaling. ERK activation in turn induces MPS degradation in a calpain-dependent manner, providing a negative feedback loop to attenuate the strength of ERK signaling. MPS degradation also leads to an increase in receptor endocytosis. Because the ligand-induced increase in the pERK signal was followed by a decay under both control conditions and conditions where the MPS degradation was inhibited by inhibiting calpain activity (Fig. 4E and fig. 15E), other MPS-independent attenuation mechanisms may contribute to the observed pERK signal decay.